metals

Article

Microstructure Evolution and Numerical Modeling of TC4 Titanium Alloy during Ultrasonic Shot Peening Process

Yuxuan Yi [1,2,3], Fei Yin [1,2,3,*], Jiajun Zhai [1,2,3] and Yanxiong Liu [1,2,3]

1 Hubei Key Laboratory of Advanced Technology for Automotive Components, Wuhan University of Technology, Wuhan 430070, China
2 School of Automotive Engineering, Wuhan University of Technology, Wuhan 430070, China
3 Hubei Longzhong Laboratory, Xiangyang 441000, China
* Correspondence: fyin@whut.edu.cn

Abstract: Ultrasonic shot peening (USP) is a surface treatment technology used in the mechanical properties strengthening of the engineering material and components during manufacturing. TC4 titanium alloy is a commonly used engineering material in the aerospace industry. In this study, a gradient nanostructured surface layer was successfully fabricated on the TC4 titanium alloy via USP technology at room temperature. The microstructure evolution of TC4 titanium alloy during USP was investigated. The surface microhardness was elevated from 330 HV to 438 HV with a penetrating depth of around 900 μm after USP with the duration of 8 min. EBSD characterization results confirmed the presence of high-density grain boundaries within the gradient structure in the region of 0–200 μm, accompanied by proliferation of dislocation density. TEM characterization indicated a substantial amount of nanograin with an average size of 74.58 nm. Furthermore, the USP process was also investigated by the finite element method to evaluate the surface-strengthening effect. The calculated maximum residual stress reached 973 MPa after multi-ball impact. The impact behavior of the shots during the USP process was studied. The effect of the parameters on the USP strengthening intensity was explored based on the validated model. This work provided a clearer understanding of the USP strengthening process of TC4 titanium alloy through an effective method of evaluating the process parameters.

Keywords: ultrasonic shot peening; surface nanocrystallization; numerical modeling; TC4 titanium alloy

Citation: Yi, Y.; Yin, F.; Zhai, J.; Liu, Y. Microstructure Evolution and Numerical Modeling of TC4 Titanium Alloy during Ultrasonic Shot Peening Process. *Metals* **2024**, *14*, 275. https://doi.org/10.3390/met14030275

Academic Editors: Judit Medina and Elvira Oñorbe

Received: 5 February 2024
Revised: 22 February 2024
Accepted: 23 February 2024
Published: 27 February 2024

1. Introduction

TC4 titanium alloy has been widely applied in many engineering fields because of its excellent mechanical properties and corrosion resistance, such as aerospace [1], automotive industries [2], biomedical engineering [3], ocean engineering [4] and so on. However, its relatively low hardness and poor wear resistance limit its practical service life and performance, resulting in a lack of reliable surface performance during application [5]. In recent years, research on surface-strengthening techniques for titanium alloys has attracted the attention of researchers worldwide to address these issues encountered in the application of TC4 titanium alloy. Past studies have proven that surface nanocrystallization (SNC) is the most effective and promising method, which induces severe plastic deformation (SPD) on the surface of metallic materials [6,7],providing a very effective potential approach for achieving microstructure refinement and enhancing the overall properties of TC4 titanium alloy. Currently, surface nanocrystallization techniques such as laser shock peening (LSP) [8–10], surface mechanical attrition treatment (SMAT) [11–13], surface mechanical rolling treatment (SMRT) [14–16], equal-channel angular pressing (ECAP) [17–19] and ultrasonic shot peening (USP) [20] are widely used to achieve grain refinement and the surface integrity enhancement of materials, aiming to improve the fatigue resistance and wear resistance of titanium alloys during service. Li et al. [21] investigated the strengthening effect of ultrasonic surface rolling at low temperatures, and demonstrated a significant enhancement of residual stress and wear properties at 120 °C. Liu et al. [22] obtained an extremely strong surface nanocrystalline layer for Ti64 after laser-assisted ultrasonic nanocrystal surface modification (LA-UNSM), showing a 75.2% increase in hardness. Kumar et al. [23] induced a surface gradient nanostructure in Ti64 alloy by ultrasonic shot peening to study the corrosion behavior of nanostructures, and the corrosion resistance showcased a great improvement after 1 min USP treatment.

Among the numerous surface nanocrystallization strengthening technologies mentioned above, USP is widely adopted and applied in the fabrication of gradient nanostructures in metallic materials. USP can strengthen the material surface with a higher intensity and hardness with the influence of an ultrasonic energy field. This leads to a core-hardening layer and rapid grain refinement, facilitating the accumulation of dislocation density within a short period of time [24–26]. In our previous work, we have successfully applied USP to the construction of gradient structures in low-carbon steel [27], 316L stainless steel [28] and M50 bearing steel [29]. We elucidated the process of structural evolution and performance enhancement of these materials at the nano scale in detail, while systematically investigating the mechanisms of their nanoscale transformation. In recent years, computer simulation has also been employed to study the correlation between process parameters and specific strengthening effects during USP. Bagherifard et al. [30] assigned the shot with motion characteristics in the form of a probability density function (PDF) to explore the random impact of the shots during USP, and the prediction for patterns of roughness, maximum residual stress (RS) and plastic strain when the shot peening coverage was carried out. Zhao et al. [31] analyzed the correlation between surface integrity after shot peening and the initial roughness of the material using a validated computational model. Ghasemi et al. [32] validated the accuracy of the finite element model using a multi-objective optimization approach and successfully predicted the parameters at which the material surface has the best surface integrity during USP treatment. However, due to the random and complex motion behavior of the balls, a simplification of maintaining a constant impact velocity was applied in the current research, without precise shot velocity measurements, to understand the energy transformation occurring after plastic deformation of the material during the USP process [33,34]. Therefore, a more accurate model is necessary for a clearer understanding and for evaluating the severe deformation process and surface-strengthening effect during the ultrasonic shot peening process.

In this study, the microstructure evolution and phase transformation of TC4 titanium alloy after USP was investigated in detail. Electron backscatter diffraction (EBSD) results showed a significant dynamic recrystallization process attributed to the microstructure refinement process. Transmission electron microscopy (TEM) results revealed that a nanocrystalline layer with the average grain size of 74.58 nm was fabricated at the top surface, resulting in great increase of 32.7% in microhardness. The impact behavior of the shot was observed with a high-speed camera. Furthermore, the finite element model (FEM) of TC4 titanium alloy during USP was established and verified. The distribution of plastic deformation and the compressive residual stress (CRS) of TC4 titanium alloy during USP was explored. This work also provided a basic evaluation of the effect of USP process parameters on the USP strengthening intensity.

2. Materials and Methods

2.1. Materials

The TC4 titanium alloy rod (Φ60 mm) used in this study was provided by Baoji Titanium Industry Co., Ltd., Baoji, China. The chemical composition of the alloy is shown in Table 1. The raw material was initially heated to 760 °C and held for 2 h before being air-cooled to room temperature. A sheet with a thickness of 4 mm was then obtained from the annealed rod through electrical discharge machining (EDM), which was then subjected to ultrasonic shot peening. The initial condition of the sheet material before USP is shown in Figure 1a–c, with the annealed TC4 coarse-grained titanium alloy primarily exhibiting a dual-phase structure of α and β phases, as confirmed by the XRD pattern at the upper right corner of Figure 1a. The IPF map in Figure 1b indicates that the average grain size of the primary structure is about 7.32 μm. The phase distribution map in Figure 1c shows that the annealed microstructure of TC4 coarse-grained titanium alloy was predominantly composed of the α phase, with a content of about 97.1%, while with a content of transformed-β phase of only 2.9%.

Table 1. Chemical compositions of TC4 titanium alloy (wt.%).

Al	V	Fe	C	N	O	Ti
6.40	4.07	0.04	0.01	0.02	0.15	Bal.

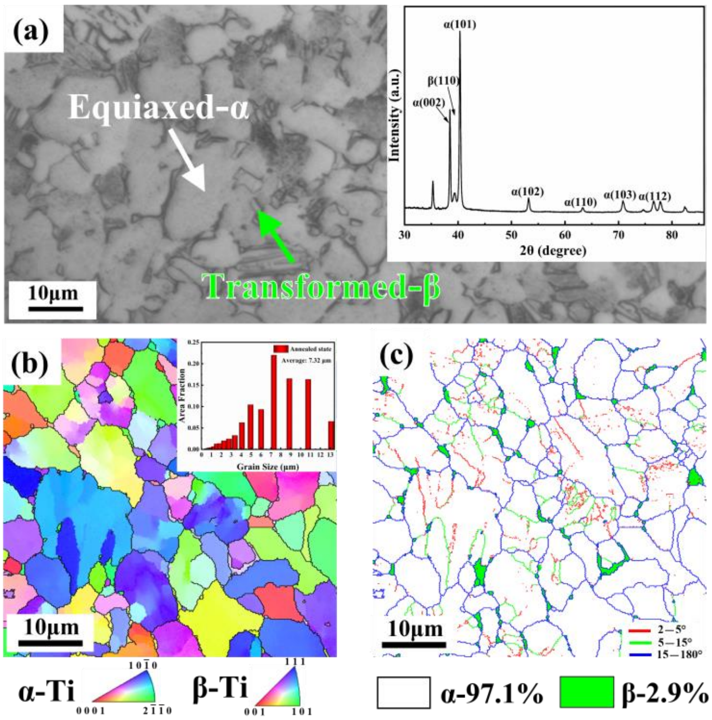

Figure 1. The initial condition of the annealed TC4 titanium alloy: (**a**) optical microscope (OM) observation and the inset XRD pattern; (**b**) IPF map; (**c**) phase distribution map.

2.2. USP Treatment

The USP treatment was conducted on a sheet material with a thickness of 4 mm at room temperature to prepare a gradient-structured TC4 titanium alloy in this study. Figure 2a depicts a schematic diagram of the USP set-up. The horn tip was made of Ti64, and its diameter was Φ26 mm. Within the closed reaction chamber, high-frequency ultrasonic waves are transduced into mechanical vibrations by the ultrasonic transducer and amplified along the axial direction, focusing high-energy vibrations onto the surface of the vibrator tip with the ultrasonic amplitude of 50 μm. Thus, twenty tungsten carbide (WC) hard alloy balls with the diameter of 4 mm and the hardness of 92 HRA (with equivalent value of 1700 HV) can be accelerated to high speed. The ultrasound wave frequency generated by the ultrasound generator is 20 kHz with a maximum output of 1.5 kW. The USP processing parameters chosen in this study were 2 min, 4 min and 8 min, respectively, with a working distance (defined as the distance from the surface of treated material to the tip of the vibrator probe) of 8.5 mm. Figure 2b gives the OM observation of the TC4 sample after USP treatment, showing that the severe plastic deformation (SPD) layer has been induced in the topmost surface of the USP-treated TC4 titanium alloy.

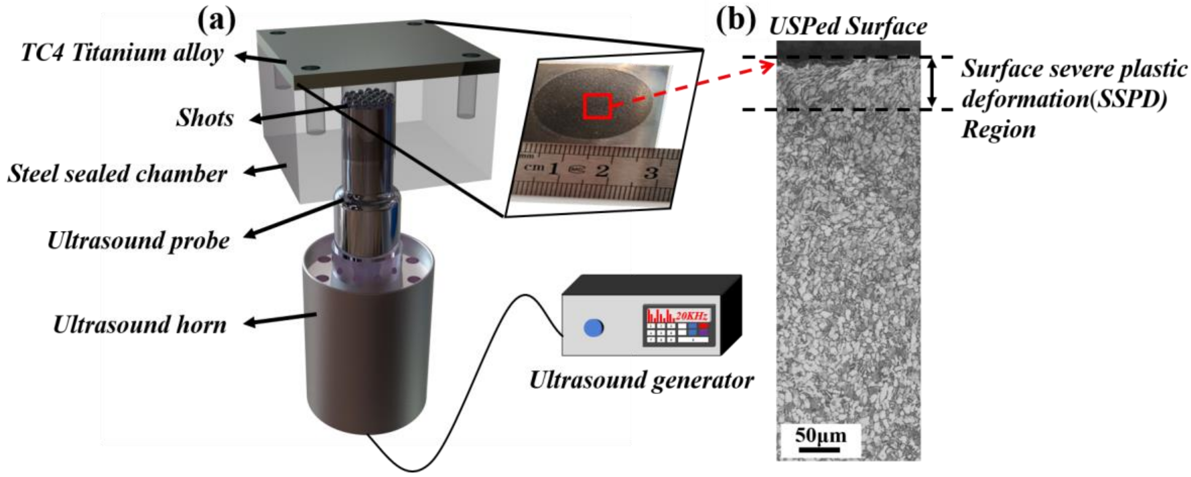

Figure 2. Schematic diagram of the USP treatment: (**a**) USP set-up; (**b**) OM observation of the USP-treated TC4 titanium alloy along its cross-sectional direction.

2.3. Measurements and Characterization

The observation of the samples after heat treatment and USP treatment was performed using a Zeiss Axio Scope A1 optical microscope. The samples before optical microscopy were mechanically ground and polished, followed by etching for 20 s in the Karlo reagent containing a volume fraction of 2% HF, 4% HNO_3 and 94% H_2O. X-ray diffraction (XRD) data were collected on the diffraction analyzer (D/MAX-RB, Rigaku, Tokyo, Japan) with a scanning speed of 1°/min. Before electron backscatter diffraction (EBSD) analysis, the samples were firstly mechanically polished and then polished using oxide polishing suspension (OPS). EBSD characterization of the cross-section structure was performed using the EDAX-TSL EBSD system installed on the FEI Quanta 450, with a scanning step size of 90 nm. The TSL OIM analysis method was employed for further analysis. To perform transmission electron microscopy (TEM) characterization, the observed surface of the TC4 sample was mechanically ground to obtain a thin slice with a thickness of 80 μm. The slices were then polished to around 25 μm on the opposite side using the Gantan 691 ion polishing system and subsequently ion-thinned. TEM characterization was carried out using the Tecnai G2 F30 with an acceleration voltage of 300 kV. Microhardness measurements were performed on each layer of the samples using the HVS-1000 Vickers hardness tester with a measurement range of 5–3000 HV after being magnified at 400 times, and with a minimum detection unit of 0.01 μm, a test force of 200 gf (1.904 N) was applied, lasting 10 s. To obtain accurate data of surface hardness, the peeling method was used to measure the depth distribution of Vickers hardness, and 10–15 points were selected randomly at each layer to record indentation on the samples subjected to grinding and polishing. The impact behavior of projectiles during the USP process was analyzed with Fastcam Nova S12 (Photron, Tokyo, Japan). Observation was carried out through a transparent acrylic chamber. The specific parameters of the camera used in the observation included a shutter speed set at 1/10,000 s and the highest image resolution of 1 K. A stable impact process lasting 1 s was captured for data analysis.

2.4. Finite Element Method

The distribution of plastic deformation and the compressive residual stress of TC4 titanium alloy during the USP process was analyzed using the FE method. The ABAQUS/CAE platform was applied to conduct the FE analysis. Considering both the simulation accuracy and efficiency, a linear hexahedral mesh was applied to the assembly model for calculations. To improve the accuracy of simulation, the minimum element size used for analysis was set to 0.06 mm. The mesh consisted of 92,792 nodes and 488,404 elements. Table 2 presents the characteristic values of the material during the elastic/plastic deformation stage in the simulated impact process. The parameters of the plastic deformation process were taken from the work by Li et al. [35]. The parameters during the elastic process were taken from the work by Xie et al. [36]. The target plate and vibrating surface was defined to be deformable and steel balls were set as rigid bodies. The effect of gravity and the interactions between balls were applied, with a Coulomb friction coefficient of 0.3. A high-frequency vibration of 20 kHz was applied to the vibrating surface using a sine function with a circular frequency. The minimum time increment was set to 1×10^{-5} s, and the total calculation time of the single-impact and multiple-impact process was 0.005 s and 0.1 s, respectively.

Table 2. Parameters for FE simulation models during the USP process.

E (GPa)	v	A (MPa)	B (MPa)	C	n	m	T_r (K)	T_m (K)
110	0.34	1098	1092	0.014	0.93	1.1	298	1878

3. Results

3.1. Gradient Nanograined Structure

3.1.1. Microstructure Evolution

To analyze the effect on the microstructure alerting of TC4 titanium alloy after USP treatment, EBSD characterization was conducted from the cross-sectional region of 0–200 µm. Figure 3a–c demonstrates a gradual refinement of the gradient microstructure on the treated surface of TC4 titanium alloy after USP process. The nanocrystalline degree increased with the prolongation of USP time, resulting in a decrease in average structural size within the region of 0–200 µm. Specifically, after an 8 min USP, the average structure size was decreased to 2.06 µm. Further statistical analysis of the average grain size in different regions in Figure 3d–g reveals that USP with a duration of 2 min was sufficient to induce a significant amount of ultrafine grain in the near-surface area of TC4 titanium alloy. When the USP time increased to 4 min, the average size within the range of 0–100 µm noticeably decreased, and the fine-grained region expanded further towards the core, while the structure size within the region of 100–200 µm underwent minimal changes as shown in Figure 3f,g. Furthermore, the decrease of grain size in this region occurred after 8 min of USP treatment, indicating a notable grain refinement in the sub-surface of the gradient nanograined structure TC4 titanium alloy.

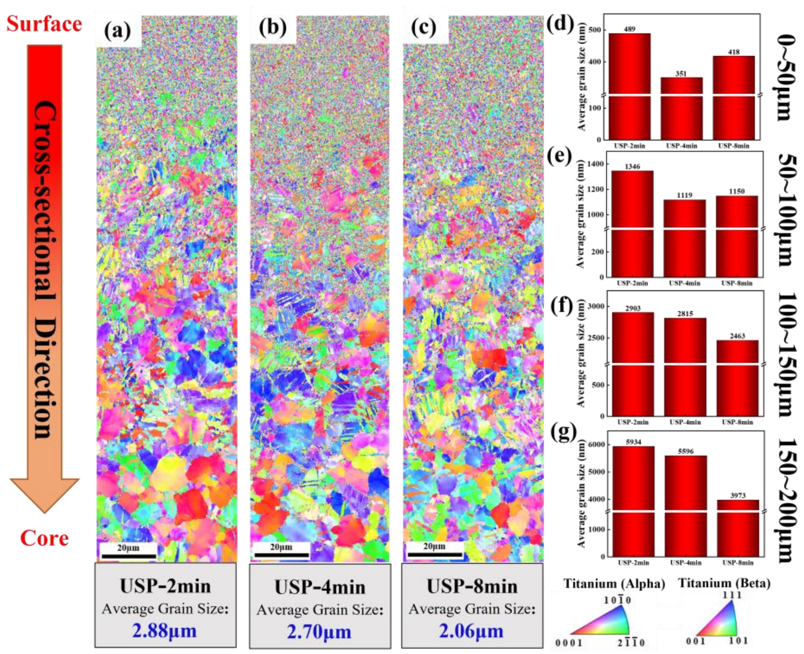

Figure 3. EBSD results of inverse pole figure (IPF) maps at the cross-sectional region of the USP-treated TC4 titanium alloy with different USP processing times: (**a**) 2 min; (**b**) 4 min; (**c**) 8 min. (**d**–**g**) average grain size statistics results for every 50 µm depth region.

3.1.2. Phase Transformation

EBSD phase maps in Figure 4a–c present the distribution and fraction change law of phase in TC4 titanium alloy at the cross-sectional region of 0–200 µm, indicating a primary α to β phase transformation within the gradient structure after USP. This deformation-induced phase transformation initiated near the USP-treated surface. The overall β phase content increased significantly from 2.9% in the initial structure to 10.2% in the 8 min USP-treated sample. Additionally, the distribution of a small amount of transformed β phase can also be observed in the region near the core. According to the statistics of β phase content in different regions in Figure 4d, a poor existent of transformed β phase was found in the region of 100–200 µm after 2 min peening duration. However, the phase transformation region gradually expanded to a deeper region as the USP time increased, and the penetrating USP energy can lead to a substantial coverage of transformed β phases within the region of 0–200 µm after 8 min of USP treatment, with an increment of β phase content in all regions.

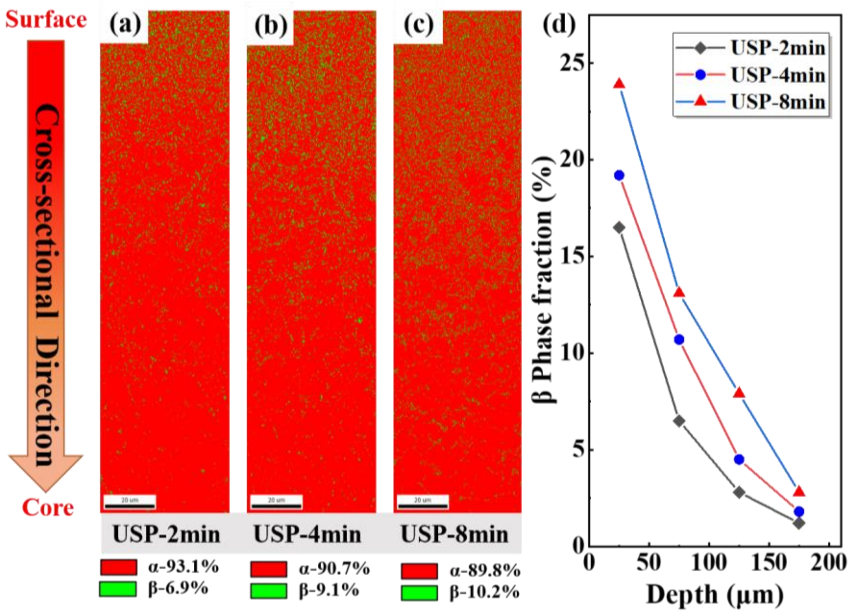

Figure 4. EBSD results of phase maps at the cross-sectional region of the USP-treated TC4 titanium alloy with different USP processing times: (**a**) 2 min; (**b**) 4 min; (**c**) 8 min. (**d**) phase fraction statistics results for every 50 µm depth region of (**a**–**c**).

3.2. Surface Nanostructure

TEM characterization at topmost surface, as showcased in Figure 5, presents a precise microstructural evolution of TC4 titanium alloy at nanoscale after 8 min USP processing. As shown in the BF image from Figure 5a, the surface microstructure was mainly composed of high-density dislocation tangles, subgrains and elongated nanograins after severe plastic deformation. The inset SAED pattern indicated the formation of a significant quantity of nanograins. The grain size statistics in dark-field images shown in Figure 5c reveals that the average grain size at surface layer was refined to 74.58 nm around after 8 min USP processing. Furthermore, the distribution of statistically stored dislocation (SSD) was characterized by HRTEM at the region in one nanograin. The SAED analysis corresponding to area I in Figure 5e confirmed that the nanostructure of the matrix was α titanium structure, and the insert IFFT image at the marked area of region A in Figure 5f indicates that a significant quantity of sawtooth-shaped dislocations appeared in the α titanium structure.

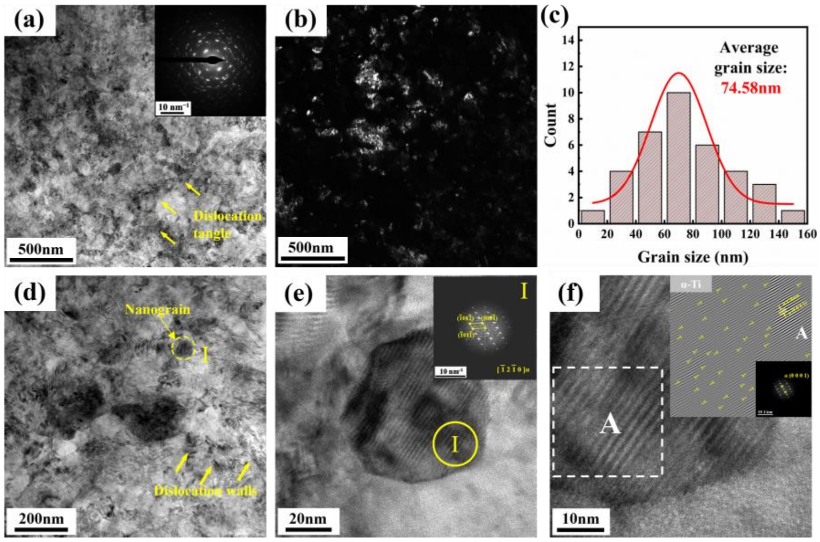

Figure 5. TEM characterization of the 8 min USP-treated TC4 titanium alloy at the treated surface: (**a**) bright-field (BF) image with SAED inset; (**b**) dark field (DF) image of the region shown in BF; (**c**) grain size statistics at the location of DF; (**d**,**e**) magnified BF images of the marked nanograin, with SAED corresponding to area I inset; (**f**) HR-TEM image of the marked area I in (**e**), with IFFT image in region A inset.

3.3. Microhardness

Figure 6 presents the distribution of microhardness with depth from the USP-treated surface of TC4 titanium alloy with different USP processing times. The hardness of untreated TC4 titanium alloy remained relatively stable at around 330 HV in different depths. After undergoing USP treatment, the surface hardness significantly increased with USP processing time, while the hardness distribution within the material exhibited a gradient descent trend. After 2 min, 4 min and 8 min of USP strengthening process, the surface hardness of TC4 titanium alloy increased to 389 HV, 413 HV and 438 HV, respectively. The USP strengthening process with 8 min duration shows the most significant increase in hardness, with a surface hardness improvement of 24.7% compared to the untreated material, and showing a hardening layer of about 900 μm.

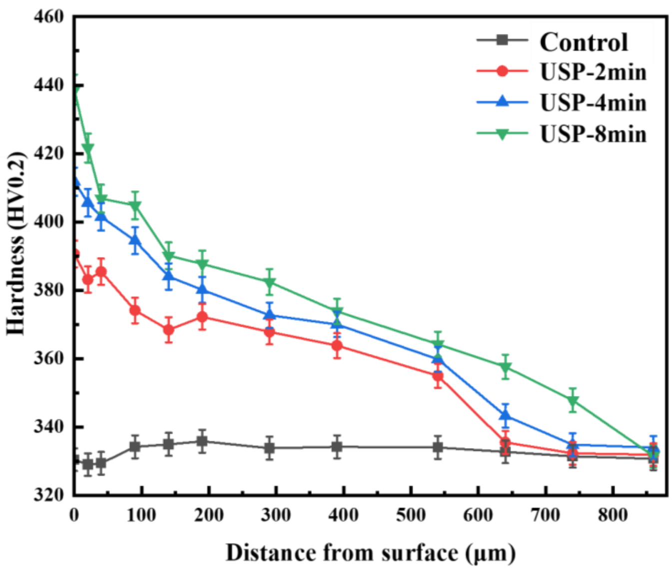

Figure 6. In-depth microhardness distribution from the USP-treated surface of TC4 titanium alloy with different USP processing times.

3.4. FEM Analysis and Motion Behavior Observation

3.4.1. Single Impact Investigation

Figure 7 shows the simulation results of a single-impact process on TC4 titanium alloy with a duration of 0.005 s during the USP process, aiming to observe and study the multiple effects induced by the USP process on the material. Figure 7a presents the planar view of the distribution of effective plastic strain on the material surface after 0.005 s of impact; four representative elements with different deformations were selected for statistical analysis in the zoomed-in image (indicated by red boxes). It can be noted from Figure 7b that the high-frequency impact of the shot can rapidly induce plastic strain on the impacted surface of the material. Figure 7d demonstrates the variation of Mises stress with shot peening time, indicating the occurrence of cumulative plastic strain accompanied by the occurrence of peak stress values, and this process only occurred after the material experienced yielding. Figure 7e illustrates the excitation velocity distribution at the surface of the vibrator tip, with a maximum vibration velocity of 6.2 m/s. Furthermore, the accumulated plastic deformation on the surface of the material occurred instantaneously during each high-speed impact of the steel ball, during which the ball velocity was rapidly reduced and reversed within a short period of time, as shown in Figure 7f. The calculated impact velocity was 10.98 m/s, while the calculated rebound velocity was 6.67 m/s on average, indicating the conversion of the impact energy into plastic work on the target material.

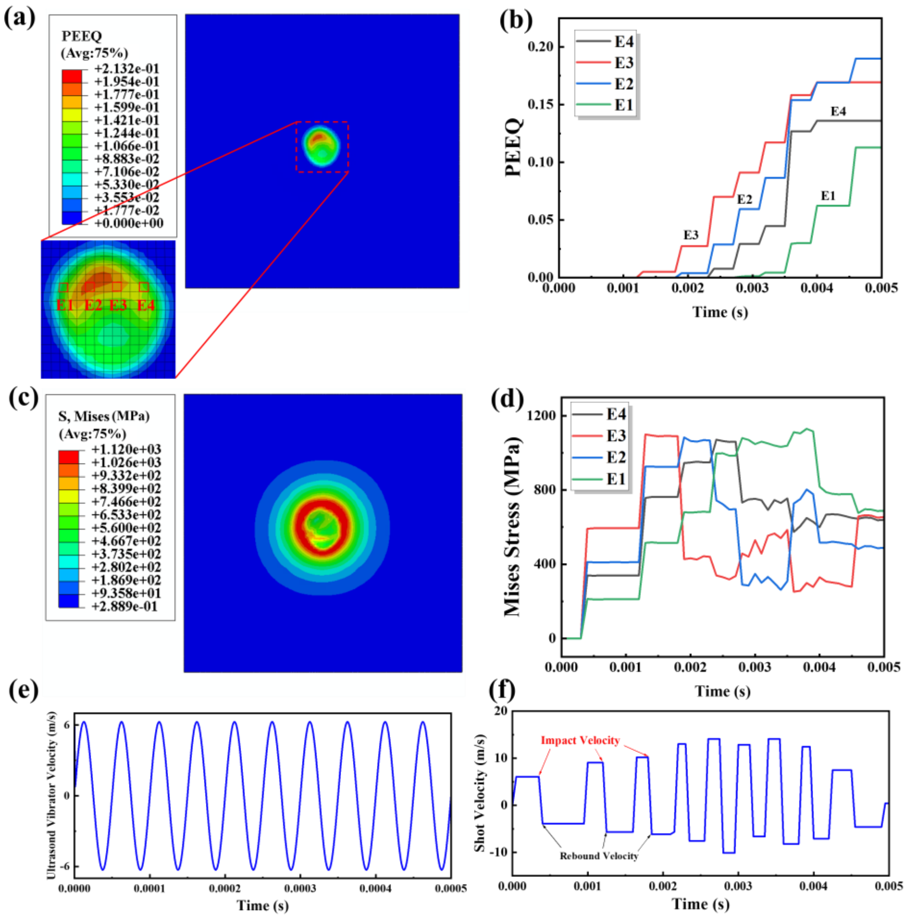

Figure 7. Simulation results of TC4 titanium alloy during USP process with single shot: (**a**) plane view of the PEEQ distribution result in the impacted surface; (**b**) variation of PEEQ with the USP processing time; (**c**) plane view of the Mises stress distribution result in the impacted surface; (**d**) variation of the Mises stress with the USP processing time; (**e**) variation of the shot velocity with the USP processing time; (**f**) ultrasound vibrator velocity variation with the USP processing time.

3.4.2. Experimental Validation of the FE Model

We obtained the surface profile changes of TC4 titanium alloy after USP processing through FEM simulation. Figure 8a demonstrates the distribution of Z-directional displacement on the target surface of TC4 titanium alloy after single-ball impact with a time span of 0.005 s. Figure 8b measures the diameter of the simulated impact crater to be 1.93 mm. These data were obtained by statistically analyzing seven consecutive node paths, as depicted by the red dots in Figure 8c. Furthermore, to compare and validate the results, we conducted measurements on five random impact craters of the material under an optical microscope, resulting in an average diameter of 1850.4 µm. This value closely matched the results from the FEM simulation, as presented in Figure 8d.

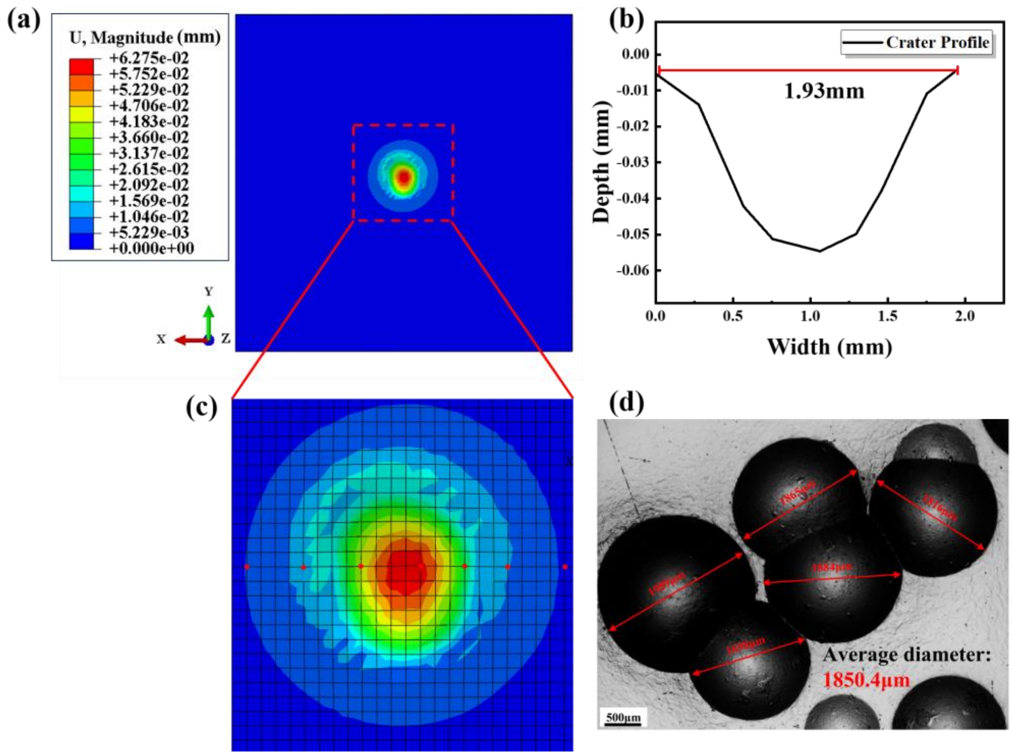

Figure 8. Surface morphology of finite element simulation and experimental observation: (**a**) the Z displacement of the peened surface of FEM result with 0.005 s period; (**b**) the measurement of the FEM crater diameter on the target surface; (**c**) magnified crater morphology of the FEM result; (**d**) optical microscopy observation of the crater's morphology on the surface of USP-treated TC4 titanium alloy.

To further validate the accuracy of the FE model, the impact behavior with single-ball during USP process was analyzed with a high-speed camera. Figure 9 shows a complete back-and-forth process captured by the high-speed camera, where four characteristic positions of the single-ball motion were extracted, including approaching the target, hitting the target, leaving the target and returning to the vibrator. Subsequently, 200 frames of stable impact during the process were selected from the video to analyze the distribution of impact velocities in detail. The velocity distribution during the stable-impact process of the single ball in the USP process is shown in Figure 10. It was found that the average impact velocity during the single-ball impact in the USP process was 10.78 m/s, while the return velocity was 6.46 m/s, which was consistent with the results obtained from the FEM analysis shown in Figure 7f.

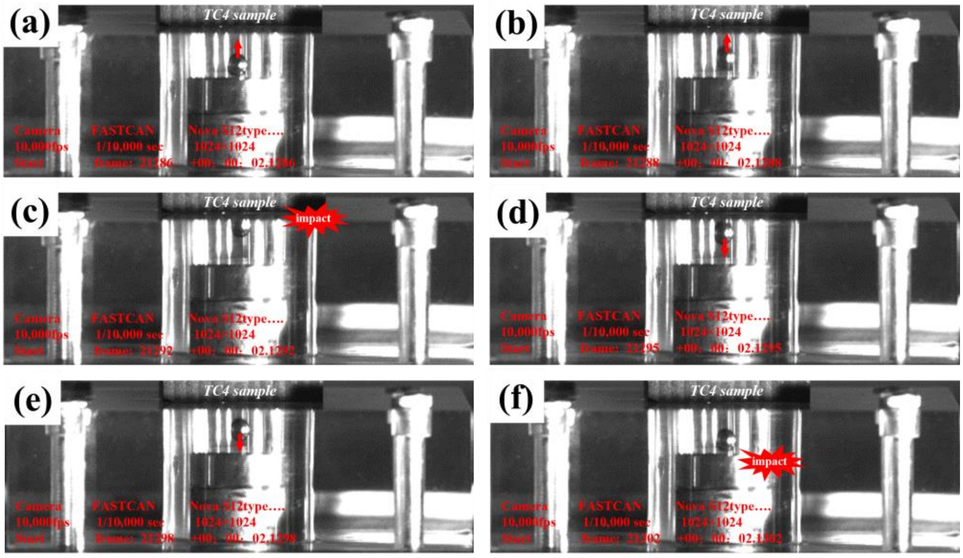

Figure 9. Observation of single-shot motion behavior during a complete back-and-forth motion process: (**a**,**b**) motion process of heading to target; (**c**) moment of hitting the target; (**d**,**e**) motion process of leaving the target; (**f**) moment of returning to the vibrator.

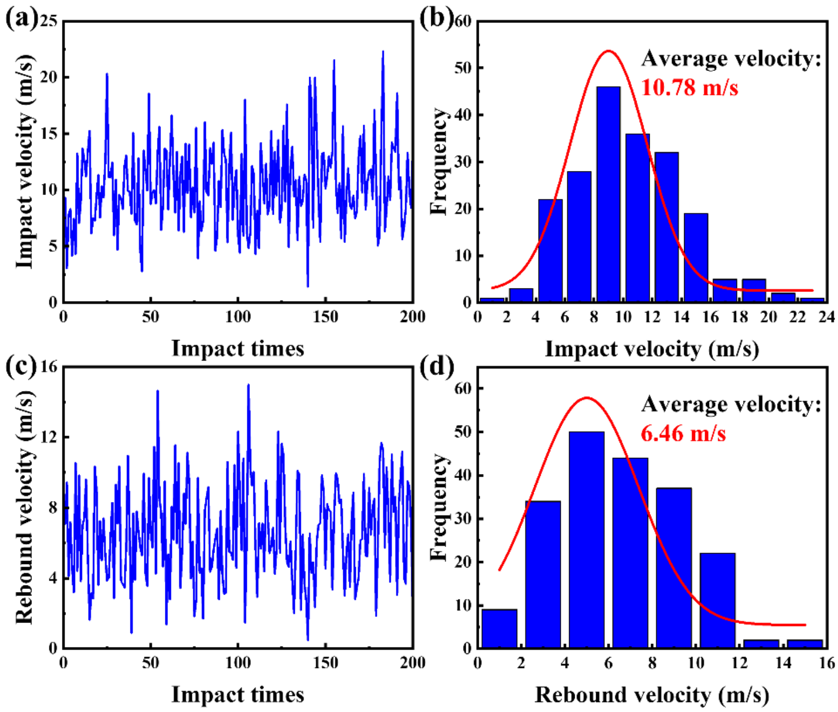

Figure 10. Velocity distribution statistics during the stable-impact period of a single ball: (**a**) statistical analysis of the impact velocities for 200 consecutive impacts; (**b**) histogram of the frequency distribution of impact velocities; (**c**) statistical analysis of return velocities for 200 consecutive impacts; (**d**) histogram of the frequency distribution of returning velocities.

3.4.3. Multiple Impacts Investigation and Observation

A notable enhancement effect of USP is the ability to generate significant residual compressive stresses in a short period of time. In order to approach the actual USP process and analyze the comprehensive effects of residual stresses and plastic strain induced by USP on TC4 titanium alloy, a multi-ball impact model consisting of five 4 mm steel balls was established. Figure 11a illustrates the schematic diagram of the FE model for the USP process under multi-ball impact, showing the gravity field, interactions between the projectiles and the sealing chamber and interactions between the projectiles. The amplitude of the vibrator tip was set at 50 μm with a vibration frequency of 20 kHz. The entire simulation process ran for about 140 h. Figure 11b highlights four prominent paths affected by residual stress after the impact. Figure 11c compares the gradient variations of the CRS (compressive residual stress) along these four paths. The simulated distribution law of residual stress in this study was highly consistent with previous work by Xie et al. [36]. The results indicate that the simulated maximum CRS value occurred in the sub-surface region of the material, with the value reaching 973 MPa. Compare Figure 11e,h, noting that the region where the maximum equivalent plastic deformation occurred on the target surface of the material coincided with the location of the maximum yield stress. Figure 11f,i illustrates the variation of stress and PEEQ over time for the five elements with severe deformation. Compared with single-shot impacts, the maximum equivalent strain on the material surface significantly increased after multiple-shot impacts. The Mises equivalent stress at the element with maximum deformation reached 1399 MPa. The plastic deformation and residual stresses at any other location on the target surface can also be accurately calculated and analyzed with this method.

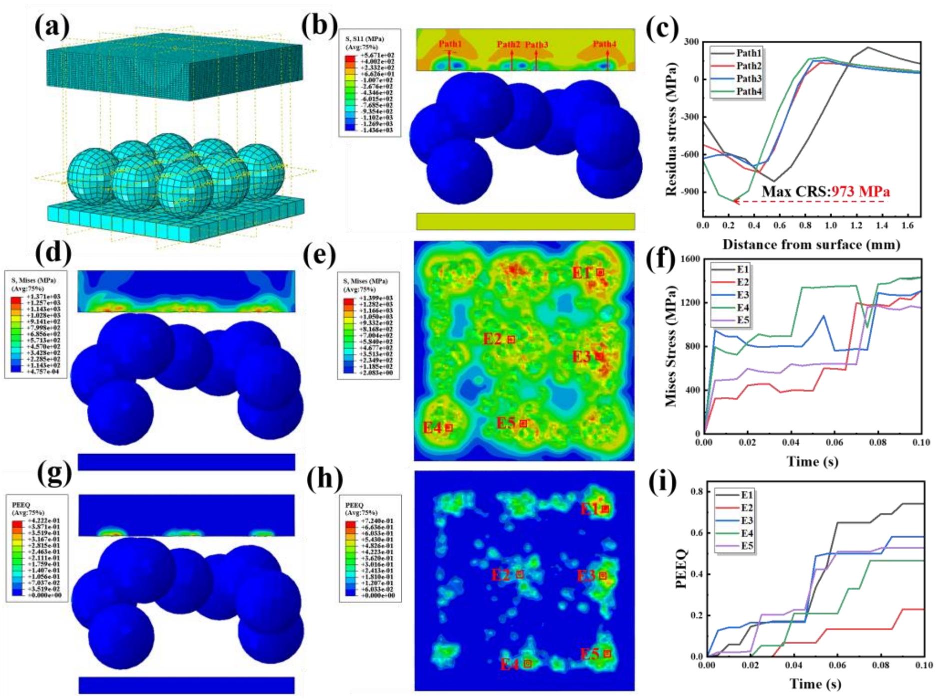

Figure 11. Simulation results of TC4 titanium alloy during USP process with multi-shots for 0.1 s duration: (**a**) the Schematic diagram of FE model; (**b**) cross-sectional view of RS distribution; (**c**) variation of RS gradient in corresponding paths; (**d**,**e**) cloud map of the Mises stress from cross-sectional view and plane view, respectively; (**f**) variation of the Mises stress with the USP processing time; (**g**,**h**) cloud map of PEEQ from cross-sectional view and plane view, respectively; (**i**) variation of PEEQ with the USP processing time.

The observation of the impact behavior with multi-shots during the USP process of TC4 titanium alloy was also conducted, as presented in Figure 12. The parameters of the high-speed camera were identical to those used for single-ball recording. Prior to the start of recording, five steel balls were evenly placed on the vibrating tip. Once the vibrator started moving, the start button of the camera was pressed. Here, six positions of the stable-impact motion of the shots were captured in every 100 frames. Through the motion pattern observation of the steel ball, we found that the interaction between balls can alter their original motion, and by influencing the number of impacts with the target material, they can increase the impact velocity. Similar phenomena have also been observed by Li et al. [37] and explained as a relay effect. While the contact interaction between the balls was not considered in their FE model, in our work, the interaction between balls in the FE model was also defined to improve the accuracy of the results.

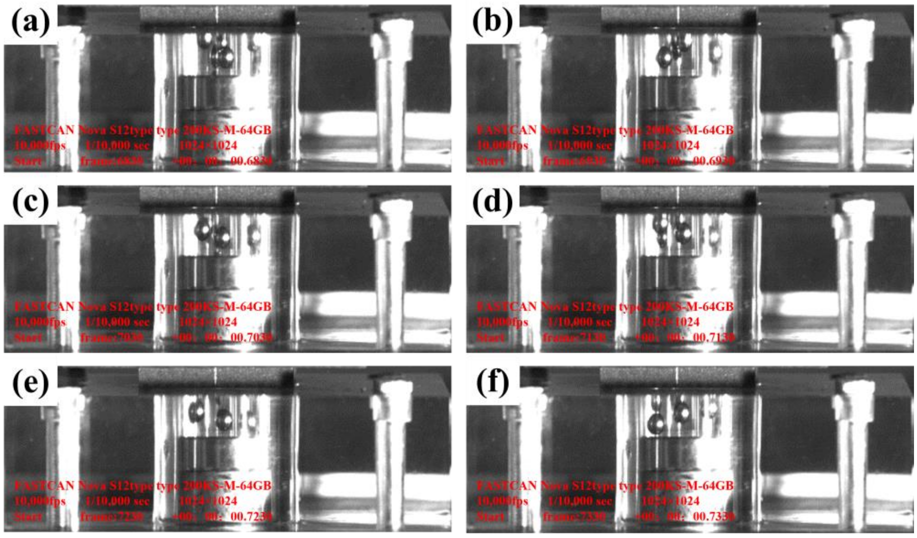

Figure 12. Observation of multi-shot's impact behavior in a consecutive impact period during USP: (**a**) the frame captured at the position of 0.6830 s; (**b**) the frame captured at the position of 0.6930 s; (**c**) the frame captured at the position of 0.7030 s; (**d**) the frame captured at the position of 0.7130 s; (**e**) the frame captured at the position of 0.7230 s; (**f**) the frame captured at the position of 0.7330 s.

4. Discussion

4.1. Microstructure Refinement Mechanism

A gradient nanograined TC4 was obtained through surface nanocrystallization by ultrasonic shot peening. Based on the statistical results of IPF in Figure 3 and TEM characterization in Figure 5, a significant structure refinement has occurred at both the treated surface and 0–200 µm region. To further investigate the microstructure refinement mechanism in materials induced by USP, the KAM distribution map in Figure 13 illustrates that the dislocation motion was initiated in the surface layer. The predominant region in blue color in the near-surface region indicates a dislocation distribution with low density in the surface layer of the TC4 titanium alloy after USP treatment. This was attributed to the high-frequency impact of balls inducing severe deforming strain in the surface layer of TC4 titanium alloy. While a relatively lower strain rate and deformation in the sub-surface enhanced the capacity of larger grains near the core to accommodate dislocations at grain boundaries, ultrasound reinforcement promoted the movement and multiplication of dislocations near the grain boundaries. Accumulation and dynamic recovery of dislocations occurred within the subgrains or dislocation cells in the surface layer. Dislocation was absorbed and low angle grain boundaries (LAGB) were consumed in a dynamic recrystallization process, leading to a transformation to high-angle grain boundaries. Figure 14 reveals that the content of LAGB within the 0–200 µm region significantly decreased after the USP process, while the content of high-angle grain boundaries (HAGB) increased significantly to 81.6%. When the accumulation of deformation-induced dislocations and dynamic recovery reached equilibrium, the microstructure was refined. Thus, a large number of ultrafine grains within the 0–50 µm range was generated, as shown in Figure 3d. Furthermore, with prolonged high-frequency impact on the material surface during USP, the gradual accumulation of high plastic strain rates led to the development of the dynamic process in the region closer to the core, resulting in further refinement of the microstructure within 100–200 µm in the 8 min USP-treated sample, as depicted in Figure 3f,g. Therefore, the degree of recrystallization significantly increased with USP processing time, as shown in Figure 14h. Overall, the nanocrystallization process was dominated by the dynamic recrystallization process in the TC4 titanium alloy.

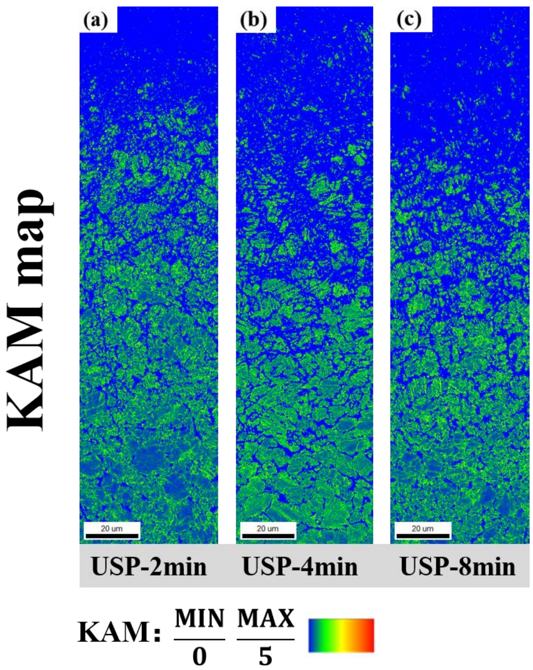

Figure 13. The kernel average misorientation (KAM) maps of the gradient nanostructured TC4 titanium alloy.

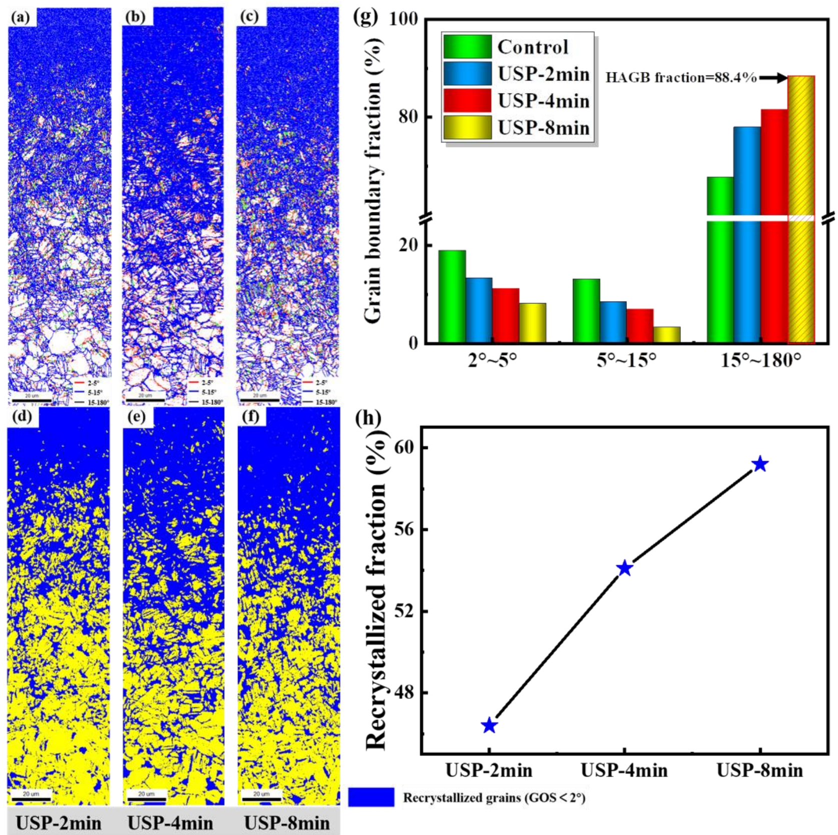

Figure 14. (**a**–**c**) grain boundary maps of the gradient nanostructured TC4 titanium alloy; (**d**–**f**) grain orientation spread (GOS) maps of the gradient nanostructured TC4 titanium alloy; (**g**) grain boundary statistics in corresponding regions of the gradient structure in (**a**–**c**); (**h**) recrystallized grain statistics in corresponding regions of the gradient structure in (**d**–**f**).

4.2. Parameter Investigation

4.2.1. Working Distance

To obtain a further evaluation of the influence of parameters on the surface-strengthening effect on TC4 titanium alloy during USP process, the variation of USP intensity with the working distance was explored. Figure 15 illustrates the influence of USP treatment on the deformation situation of TC4 titanium alloy when controlling other parameters while varying the working distance. With the reduction of working distance, there was a significant increase in the maximum Mises stress. The deformation zone expanded within the surface layer of the TC4 material. As shown in Figure 15(d3), the accumulated plastic deformation exhibited a significant decrease with the working distance, which was attributed to the increased times of effective impacts resulting from the shorter working distance. Thus, the reduction of working distance resulted in rapid accumulation of effective plastic strain.

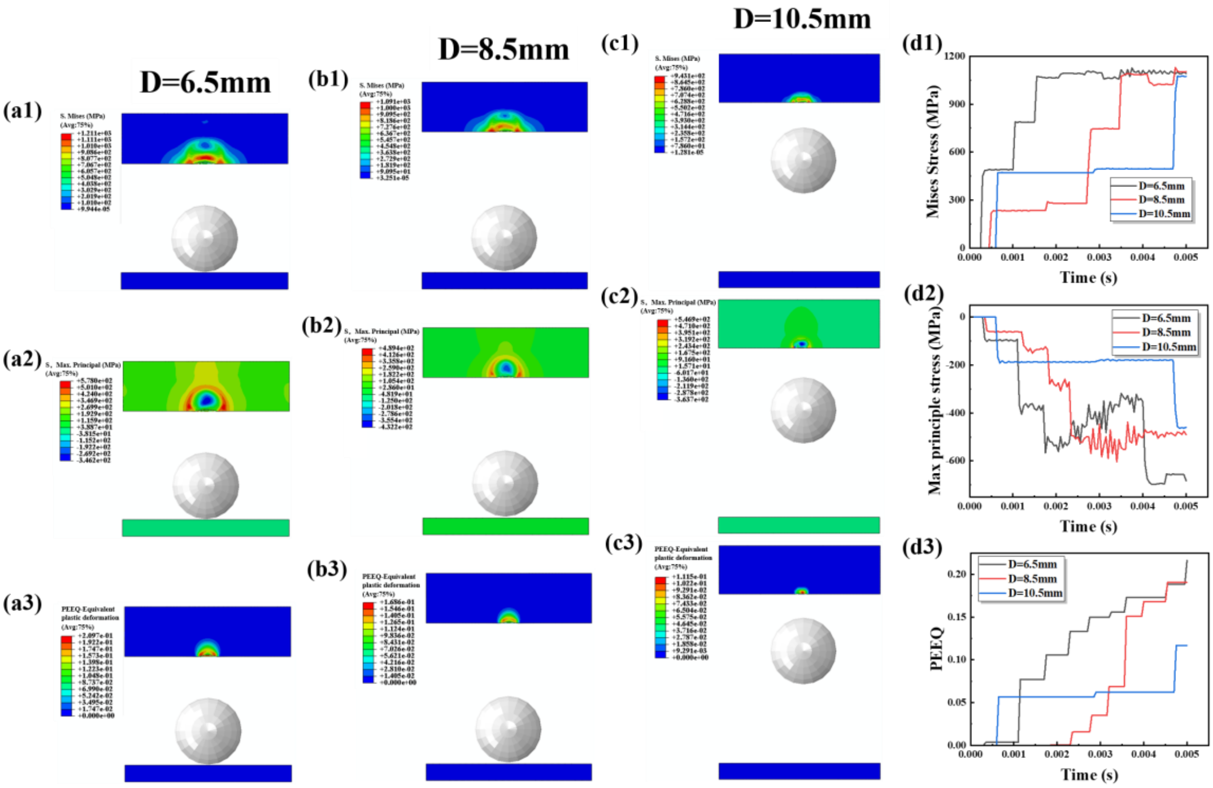

Figure 15. Effect of working distance on the plastic deformation of TC4 titanium alloy during the USP process: (**a1**–**a3**) FEM cloud map from cross-sectional view of Mises stress, maximum principal stress and PEEQ at the working distance of 6.5 µm; (**b1**–**b3**) FEM cloud map from cross-sectional view of Mises stress, maximum principal stress and PEEQ at the working distance of 8.5 µm; (**c1**–**c3**) FEM cloud map from cross-sectional view of Mises stress, maximum principal stress and PEEQ at the working distance of 10.5 µm; (**d1**–**d3**) variation patterns of plastic deformation parameters with working distance in the USP process.

4.2.2. Ultrasound Frequency

The variation of peening intensity with the ultrasound frequency was investigated. Figure 16 shows the influence of USP treatment on the deformation situation of TC4 titanium alloy by altering the ultrasonic frequency when controlling other parameters. With the increment of ultrasonic frequency, the plastic deformation and compressive stress significantly increase within the same processing time. Simultaneously, larger plastic deformation regions and compressive stress areas were induced on the target surface. This indicates that appropriately adjusting the frequency of ultrasonic vibration within a certain range can rapidly and effectively enhance the strengthening intensity of materials.

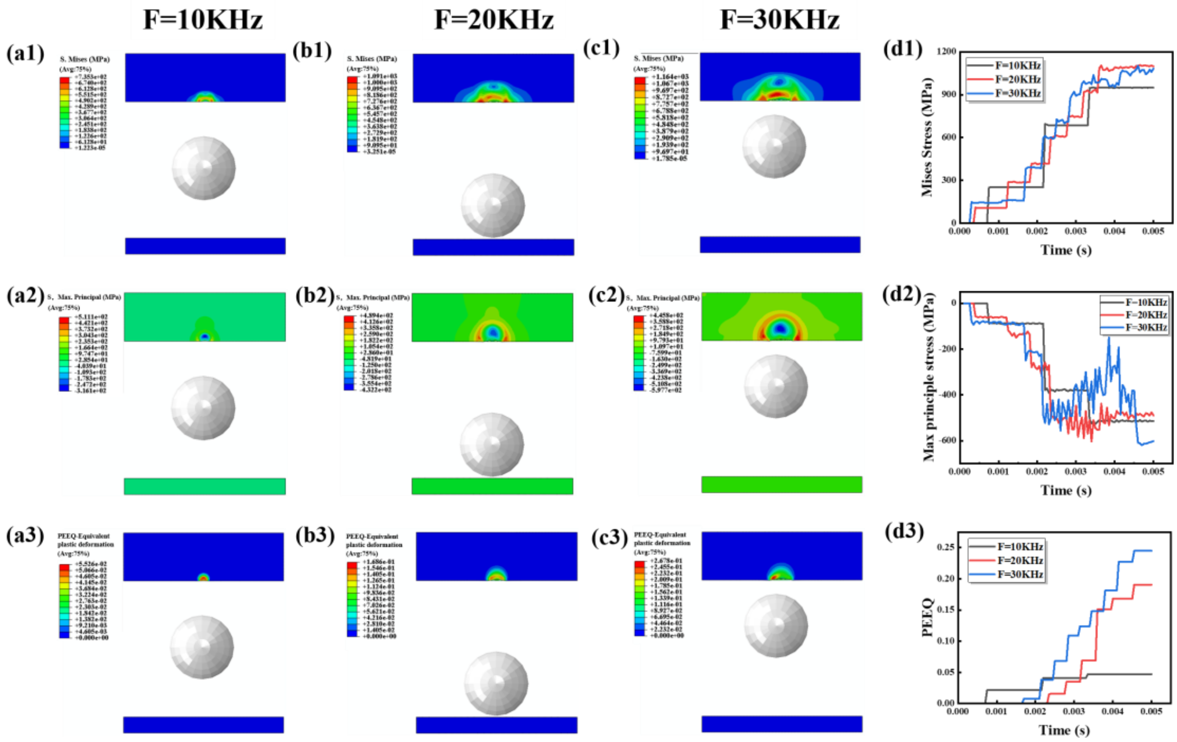

Figure 16. Effect of ultrasound frequency on the plastic deformation of TC4 titanium alloy during the USP process: (**a1**–**a3**) FEM cloud map from cross-sectional view of von Mises stress, maximum principal stress and PEEQ with the ultrasound frequency of 10 kHz; (**b1**–**b3**) FEM cloud map from cross-sectional view of Mises stress, maximum principal stress and PEEQ with the ultrasound frequency of 20 kHz; (**c1**–**c3**) FEM cloud map from cross-sectional view of Mises stress, maximum principal stress and PEEQ with the ultrasound frequency of 30 kHz; (**d1**–**d3**) variation patterns of plastic deformation parameters with ultrasonic frequency in the USP process.

4.2.3. Ultrasound Amplitude

The variation of peening intensity with the ultrasound amplitude during USP was explored. Figure 17 shows the distribution and variation patterns of plastic deformation parameters with ultrasound amplitude in the USP process. The maximum PEEQ value increased from 0.06226 to 0.2887 with increased ultrasonic amplitude. Both the magnitude of the equivalent stress and the degree of plastic deformation have significantly improved with the increase of ultrasonic amplitude. This can be attributed to the increment in ultrasound amplitude inducing greater kinetic energy and thus motivating the ball within a short time, indirectly increasing the impact time of shot and intensity of impacts. Adjusting the ultrasonic amplitude appropriately is an effective means to enhance the intensity of USP processing.

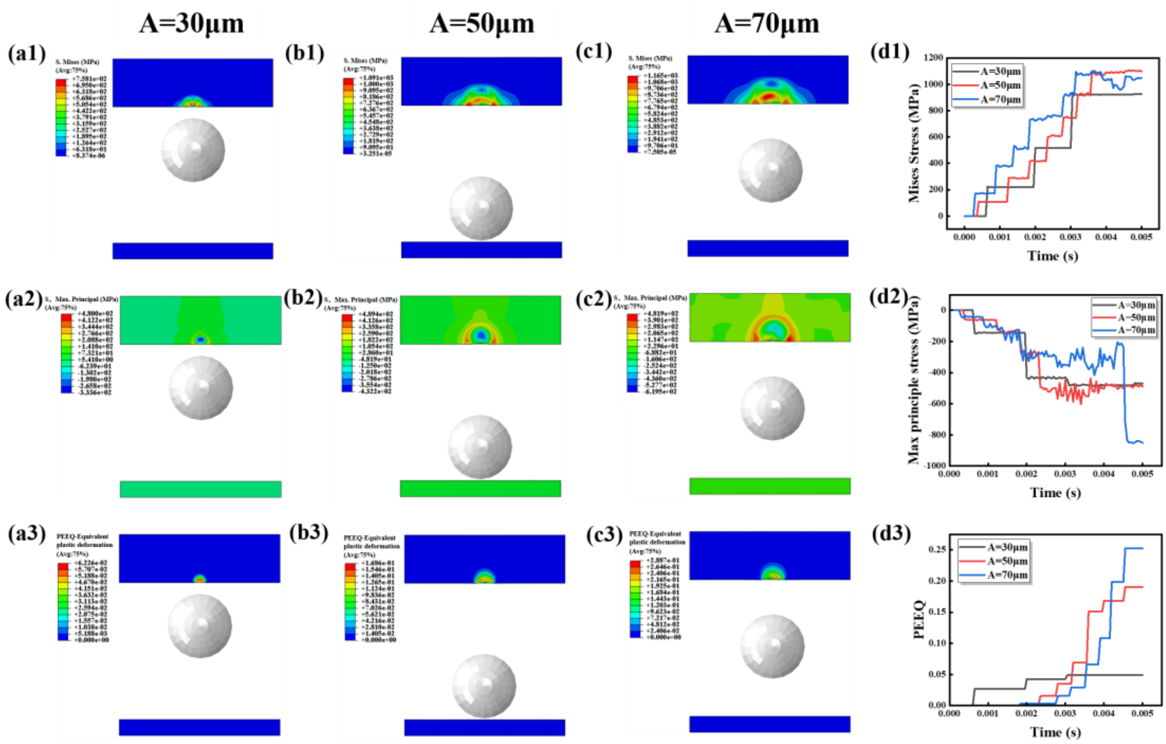

Figure 17. Effect of ultrasound amplitude on the plastic deformation of TC4 titanium alloy during the USP process: (**a1**–**a3**) FEM cloud map from cross-sectional view of Mises stress, maximum principal stress and PEEQ with the ultrasound amplitude of 30 μm; (**b1**–**b3**) FEM cloud map from cross-sectional view of Mises stress, maximum principal stress and PEEQ with the ultrasound amplitude of 50 μm; (**c1**–**c3**) FEM cloud map from cross-sectional view of Mises stress, maximum principal stress and PEEQ with the ultrasound amplitude of 70 μm; (**d1**–**d3**) variation of Mises stress, maximum principal stress and PEEQ with USP ultrasound amplitude.

5. Conclusions

In this study, we successfully prepared gradient nanostructured TC4 titanium alloy using the ultrasonic shot peening (USP) technique. The surface nanocrystallization and dynamic recrystallization processes during USP were discussed. The process of single-ball and multi-ball impact in ultrasonic shot peening was simulated using a finite element method, and the model was validated through experiments. The effects of USP process parameters on the strengthening effect were analyzed. The following conclusions can be drawn:

(1) After 8 min of USP, significant microstructural refinement and the β phase transformation occurred in the material within the region of 0–200 μm. A significant quantity of nanograins formed on the treated surface, accompanied by abundant dislocation generation. The grain size on the peened surface decreased from 7.32 μm to 74.58 nm, and the surface microhardness increased from 330 HV to 438 HV.

(2) The dynamic recrystallization process dominated the nanocrystallization process by inducing consecutive severe plastic deformation in the titanium alloy. The recrystallization degree increased after the USP process. The accumulation of high plastic strain rates on the treated surface by USP resulted in an increase of dislocation density and formation of grain boundaries within the region of 0–200 μm.

(3) The plastic deformation distribution during single-ball and multi-ball impact processes was calculated via FEM. The FE simulation results agreed well with the experimental results. The simulated maximum CRS in the sub-surface reached 973 MPa after multi-ball impact.

(4) The impact behavior of the shots during the USP process was analyzed. The experimental observations validated the accuracy of the model. The strengthening intensity

of USP was improved with the USP parameters of working distance, ultrasonic frequency and amplitude based on the validated model.

Author Contributions: Conceptualization, F.Y. and Y.L.; methodology, Y.Y.; software, J.Z.; validation, F.Y., Y.Y. and J.Z.; formal analysis, Y.Y.; investigation, Y.Y.; resources, Y.L.; data curation, Y.Y.; writing—original draft preparation, Y.Y.; writing—review and editing, F.Y.; visualization, F.Y.; supervision, Y.L.; project administration, F.Y.; funding acquisition, F.Y. All authors have read and agreed to the published version of the manuscript.

Funding: This work was financially supported by the National Key R&D Program of China (No. 2020YFA0714900), Science and Technology Innovation Talents and Service Project of Hubei Province (2022EJD012), Independent Innovation Projects of the Hubei Longzhong Laboratory (2022ZZ-26), National Natural Science Foundation of China (No. 51975441), Fundamental Research Funds for the Central Universities (WUT: 2020IVA020), Overseas Expertise Introduction Project for Discipline Innovation (B17034), and Innovative Research Team Development Program of the Ministry of Education of China (IRT_17R83).

Data Availability Statement: The raw data supporting the conclusions of this article will be made available by the authors on request.

Conflicts of Interest: The authors declare no conflicts of interest.

References

1. Boyer, R.R. An overview on the use of titanium in the aerospace industry. *Mater. Sci. Eng. A* **1996**, *213*, 103–114. [CrossRef]
2. Sachdev, A.K.; Kulkarni, K.; Fang, Z.Z.; Yang, R.; Girshov, V. Titanium for Automotive Applications: Challenges and Opportunities in Materials and Processing. *JOM* **2012**, *64*, 553–565. [CrossRef]
3. Sidambe, A. Biocompatibility of Advanced Manufactured Titanium Implants—A Review. *Materials* **2014**, *7*, 8168–8188. [CrossRef] [PubMed]
4. Cheng, J.; Li, F.; Zhu, S.; Yu, Y.; Qiao, Z.; Yang, J. Electrochemical corrosion and tribological evaluation of TiAl alloy for marine application. *Tribol. Int.* **2017**, *115*, 483–492. [CrossRef]
5. Liu, Y.G.; Li, M.Q.; Liu, H.J. Surface nanocrystallization and gradient structure developed in the bulk TC4 alloy processed by shot peening. *J. Alloys Compd.* **2016**, *685*, 186–193. [CrossRef]
6. Yin, F.; Hu, S.; Xu, R.; Han, X.; Qian, D.; Wei, W.; Hua, L.; Zhao, K. Strain rate sensitivity of the ultrastrong gradient nanocrystalline 316L stainless steel and its rate-dependent modeling at nanoscale. *Int. J. Plast.* **2020**, *129*, 102696. [CrossRef]
7. Fan, K.; Liu, D.; Wang, C.; Yang, J.; Liu, Y.; Zhang, X.; Xiang, J.; Abdel Wahab, M. Effect of contact stress and slip amplitude on fretting fatigue behaviour of ultrasonic surface nanocrystallized TC11 titanium alloy. *J. Mater. Res. Technol.* **2024**, *28*, 4052–4064. [CrossRef]
8. Li, L.; Jia, W.; Ji, V. Phase transformations mechanism in commercially pure titanium subjected to multiple laser shock peening. *Surf. Coat. Technol.* **2022**, *450*, 129010. [CrossRef]
9. He, D.; Li, L.; Zhang, Y.; Chi, J.; Zhang, H.; Rujian, S.; Che, Z.; Zhang, H.; Guo, W. Gradient Microstructure and Fatigue Properties of TC21 Titanium Alloy Processed by Laser Shock Peening. *J. Alloys Compd.* **2022**, *935*, 168139. [CrossRef]
10. Nalla, R.K.; Altenberger, I.; Noster, U.; Liu, G.Y.; Scholtes, B.; Ritchie, R.O. On the influence of mechanical surface treatments—Deep rolling and laser shock peening—On the fatigue behavior of Ti–6Al–4V at ambient and elevated temperatures. *Mater. Sci. Eng. A* **2003**, *355*, 216–230. [CrossRef]
11. Sami, J.; Richard, C.; Retraint, D.; Roland, T.; Chemkhi, M.; Demangel, C. Effect of surface nanocrystallization on the corrosion behavior of Ti–6Al–4V titanium alloy. *Surf. Coat. Technol.* **2013**, *224*, 82–87. [CrossRef]
12. Bahl, S.; Suwas, S.; Ungàr, T.; Chatterjee, K. Elucidating microstructural evolution and strengthening mechanisms in nanocrystalline surface induced by surface mechanical attrition treatment of stainless steel. *Acta Mater.* **2017**, *122*, 138–151. [CrossRef]
13. Wei, P.; Hua, P.; Xia, M.; Yan, K.; Lin, H.; Yi, S.; Lu, J.; Ren, F.; Sun, Q. Bending fatigue life enhancement of NiTi alloy by pre-strain warm surface mechanical attrition treatment. *Acta Mater.* **2022**, *240*, 118269. [CrossRef]
14. Wang, C.; Liu, X.; Hu, X.; Fei, S.; Li, B.; Deng, H.; Shen, G.; Wang, X. Gradient-structured 1060 aluminum by air pressure-driven surface mechanical rolling treatment and its effects on the friction performance. *J. Manuf. Process.* **2023**, *108*, 804–819. [CrossRef]
15. Carneiro, L.; Wang, X.; Jiang, Y. Cyclic deformation and fatigue behavior of 316L stainless steel processed by surface mechanical rolling treatment. *Int. J. Fatigue* **2020**, *134*, 105469. [CrossRef]
16. Zhu, R.; Ma, S.; Wang, X.; Chen, J.; Pengfei, H.; Wang, Y. Effect of ultrasonic surface rolling process on hydrogen embrittlement behavior of TC4 laser welded joints. *J. Mater. Sci.* **2022**, *57*, 11997–12011. [CrossRef]
17. Berezin, I.; Zalazinsky, A.; Kryuchkov, D. Analytical model of equal-channel angular pressing of titanium sponge. *Met. Work. Mater. Sci.* **2023**, *25*, 17–31. [CrossRef]
18. Jia, D.-S.; He, T.; Song, M.; Huo, Y.-M.; Hu, H.-Y. Effects of equal channel angular pressing and further cold upsetting process to the kinetics of precipitation during aging of 7050 aluminum alloy. *J. Mater. Res. Technol.* **2023**, *26*, 5126–5140. [CrossRef]

19. Zhang, B.; Chen, Y.; Yang, Y.; Gu, H.; You, H. Improving Mechanical Properties, Corrosion Resistance and Biocompatibility of Zn-1Mg-0.3Y Alloys Through Equal Channel Angular Pressing. *Sci. Adv. Mater.* **2023**, *15*, 1328–1335. [CrossRef]
20. Li, Y.; Liu, X.; Wang, F.; Zhou, W.; Ren, X. Influence of ultrasonic shot peening on the surface acid etching behavior of pure titanium. *Mater. Chem. Phys.* **2024**, *313*, 128720. [CrossRef]
21. Li, G.; Qu, S.; Xie, M.; Li, X. Effect of ultrasonic surface rolling at low temperatures on surface layer microstructure and properties of HIP Ti-6Al-4V alloy. *Surf. Coat. Technol.* **2017**, *316*, 75–84. [CrossRef]
22. Liu, J.; Suslov, S.; Ren, Z.; Dong, Y.; Ye, C. Microstructure Evolution in Ti64 Subjected to Laser-assisted Ultrasonic Nanocrystal Surface Modification. *Int. J. Mach. Tools Manuf.* **2018**, *136*, 19–33. [CrossRef]
23. Kumar, S.; Chattopadhyay, K.; Singh, V. Effect of surface nanostructuring on corrosion behavior of Ti-6Al-4V alloy. *Mater. Charact.* **2016**, *121*, 23–30. [CrossRef]
24. Han, M.; Du, J.; Chen, Y.; Sun, Q.; Hu, K. Influence of ultrasonic shot peening on the microstructure and corrosion behavior of AZ80M magnesium alloy. *J. Alloys Compd.* **2024**, *980*, 173633. [CrossRef]
25. Malaki, M.; Ding, H. A review of ultrasonic peening treatment. *Mater. Des.* **2015**, *87*, 1072–1086. [CrossRef]
26. Sun, Q.; Han, Q.; Wang, S.; Xu, R. Microstructure, corrosion behaviour and thermal stability of AA 7150 after ultrasonic shot peening. *Surf. Coat. Technol.* **2020**, *398*, 126127. [CrossRef]
27. Yin, F.; Hu, S.; Hua, L.; Wang, X.; Suslov, S.; Han, Q. Surface Nanocrystallization and Numerical Modeling of Low Carbon Steel by Means of Ultrasonic Shot Peening. *Metall. Mater. Trans. A* **2014**, *46*, 1253–1261. [CrossRef]
28. Yin, F.; Cheng, G.; Xu, R.; Zhao, K.; Li, Q.; Jian, J.; Hu, S.; Sun, S.; An, L.; Han, Q. Ultrastrong nanocrystalline stainless steel and its Hall-Petch relationship in the nanoscale. *Scr. Mater.* **2018**, *155*, 26–31. [CrossRef]
29. Yue, X.; Hu, S.; Wang, X.; Liu, Y.; Yin, F.; Hua, L. Understanding the nanostructure evolution and the mechanical strengthening of the M50 bearing steel during ultrasonic shot peening. *Mater. Sci. Eng. A* **2022**, *836*, 142721. [CrossRef]
30. Bagherifard, S.; Ghelichi, R.; Guagliano, M. Numerical and experimental analysis of surface roughness generated by shot peening. *Appl. Surf. Sci.* **2012**, *258*, 6831–6840. [CrossRef]
31. Jiuyue, Z.; Tang, J.; Zhou, W.; Jiang, T.; Liu, H.; Xing, B. Numerical modeling and experimental verification of residual stress distribution evolution of 12Cr2Ni4A steel generated by shot peening. *Surf. Coat. Technol.* **2021**, *430*, 127993. [CrossRef]
32. Ghasemi, A.; Vanini, S.A.S. A comprehensive investigation on the effect of controlling parameters of ultrasonic peening treatment on residual stress and surface roughness: Experiments, numerical simulations and optimization. *Surf. Coat. Technol.* **2023**, *464*, 129515. [CrossRef]
33. Zhang, B.; Liu, H.; Bai, H.; Zhu, C.; Wu, W. Ratchetting–multiaxial fatigue damage analysis in gear rolling contact considering tooth surface roughness. *Wear* **2019**, *428–429*, 137–146. [CrossRef]
34. Lin, Q.; Liu, H.; Zhu, C.; Parker, R.G. Investigation on the effect of shot peening coverage on the surface integrity. *Appl. Surf. Sci.* **2019**, *489*, 66–72. [CrossRef]
35. Li, K.; Wang, C.; Hu, X.; Zhou, Y.; Lai, Y.; Wang, C. DEM-FEM coupling simulation of residual stresses and surface roughness induced by shot peening of TC4 titanium alloy. *Int. J. Adv. Manuf. Technol.* **2022**, *118*, 1469–1483. [CrossRef]
36. Xie, L.; Zhang, J.; Xiong, C.; Wu, L.; Jiang, C.; Lu, W. Investigation on experiments and numerical modelling of the residual stress distribution in deformed surface layer of Ti–6Al–4V after shot peening. *Mater. Des.* **2012**, *41*, 314–318. [CrossRef]
37. Li, P.; Hu, S.; Liu, Y.; Hua, L.; Yin, F. Surface Nanocrystallization and Numerical Modeling of 316L Stainless Steel during Ultrasonic Shot Peening Process. *Metals* **2022**, *12*, 1673. [CrossRef]